

PAMOP: Petascale Atomic, Molecular and Optical Collision Calculations

B M McLaughlin, C P Ballance, M S Pindzola and A Müller

Abstract Petaflop architectures are currently being utilized efficiently to perform large scale computations in Atomic, Molecular and Optical Collisions. We solve the Schrödinger or Dirac equation for the appropriate collision problem using the R-matrix or R-matrix with pseudo-states approach. We briefly outline the parallel methodology used and implemented for the current suite of Breit-Pauli and DARC codes. In this report, various examples are shown of our theoretical results compared with experimental results obtained from Synchrotron Radiation facilities where the Cray architecture at HLRS is playing an integral part in our computational projects.

1 Introduction

Our research efforts continue to focus on the development of computational methods to solve the Schrödinger and Dirac equations for atomic and molecular collision processes. Access to leadership-class computers such as the Cray XE6 at HLRS allows us to benchmark our theoretical solutions against dedicated collision exper-

B M McLaughlin

Centre for Theoretical Atomic, Molecular and Optical Physics (CTAMOP), School of Mathematics & Physics, The David Bates Building, Queen's University, 7 College Park, Belfast BT7 1NN, UK, e-mail: b.mclaughlin@qub.ac.uk

C P Ballance

Department of Physics, 206 Allison Laboratory, Auburn University, Auburn, AL 36849, USA e-mail: ballance@physics.auburn.edu

M S Pindzola

Department of Physics, 206 Allison Laboratory, Auburn University, Auburn, AL 36849, USA e-mail: pindzola@physics.auburn.edu

A Müller

Institut für Atom- und Molekülphysik, Justus-Liebig-Universität Giessen, 35392 Giessen, Germany e-mail: Alfred.Mueller@iamp.physik.uni-giessen.de

iments at synchrotron facilities such as the Advanced Light Source (ALS), Astrid II, BESSY II, SOLEIL and Petra III and to provide atomic and molecular data for ongoing research in laboratory and astrophysical plasma science. In order to have direct comparisons with experiment, semi-relativistic or fully relativistic computations, involving a large number of target-coupled states are required to achieve spectroscopic accuracy. These computations could not be even attempted without access to HPC resources such as those available at leadership computational centers in Europe (HLRS) and the USA (NERSC, NICS and ORNL). We use the R-matrix and R-matrix with pseudo-states (RMPS) methods to solve the Schrödinger and Dirac equations for atomic and molecular collision processes.

Satellites such as *Chandra* and *XMM-Newton* are currently providing a wealth of X-ray spectra on many astronomical objects, but a serious lack of adequate atomic data, particularly in the *K*-shell energy range, impedes the interpretation of these spectra. Spectroscopy in the soft X-ray region (0.5–4.5 nm), including *K*-shell transitions of singly and multiply charged ionic forms of atomic elements such as Be, B, C, N, O, Ne, S and Si, as well as L-shell transitions of Fe and Ni, provides a valuable probe of the extreme environments in astrophysical sources such as active galactic nuclei (AGN's), X-ray binary systems, and cataclysmic variables [1, 2, 3]. For example, *K*-shell photoabsorption cross sections for the carbon isonuclear sequence have been used to model the Chandra X-ray absorption spectrum of the bright blazar Mkn 421 [4].

The motivation for our work is multi-fold; (a) Astrophysical Applications [4, 9], (b) Fusion and plasma modelling, JET, ITER, (c) Fundamental interest and (d) Support of experimental measurements and Satellite observations. In the case of heavy atomic systems [5, 12], little atomic data exists and our work provides results for new frontiers on the application of the R-matrix; Breit-Pauli and DARC parallel suite of codes. Our highly efficient R-matrix codes are widely applicable to the support of present experiments being performed at synchrotron radiations facilities such as; ALS, ASTRID II, SOLEIL, PETRA III, BESSY II. Various examples of large scale calculations are presented to illustrate the predictive nature of the method.

The main question asked of any method is, how do we deal with the many body problem? In our case we use first principle methods (ab initio) to solve our dynamical equations of motion. Ab initio methods provide highly accurate, reliable atomic and molecular data (using state-of-the-art techniques) for solving the Schrödinger and Dirac equation. The R-matrix non-perturbative method is used to model accurately a wide variety of atomic, molecular and optical processes such as; electron impact ionization (EII), electron impact excitation (EIE), single and double photoionization and inner-shell X-ray processes. The R-matrix method provides highly accurate cross sections and rates used as input for astrophysical modeling codes such as; CLOUDY, CHIANTI, AtomDB, XSTAR necessary for interpreting experiment/satellite observations of astrophysical objects and fusion and plasma modeling for JET and ITER.

2 Parallel R-matrix Photoionization

The use of massively parallel architectures allows one to attempt calculations which previously could not have been addressed. This approach enables large scale relativistic calculations for trans-iron elements such as ; Kr-ions, Xe-ions [5] and W-ions [6, 7]. It allows one to provide atomic data in the absence of experiment and takes advantage of the linear algebra libraries available on most architectures. We fill in our sea of ignorance i.e. provide data on atomic elements where none have previously existed. The present approach has the capability to cater for Hamiltonian matrices in excess of $250 \text{ K} \times 250 \text{ K}$. Examples are presented for both valence and inner-shell photoionization for systems of prime interest to astrophysics and for complex species necessary for plasma modeling in fusion tokamaks.

The development of the dipole codes benefit from similar modifications and developments made to the existing excitation R-matrix codes. In this case all the eigenvectors from a pair of dipole allowed symmetries are required for bound-free dipole matrix formation. Every dipole matrix pair is carried out concurrently with groups of processors assigned to an individual dipole. The method is applicable to photoionization, dielectronic-recombination or radiation damped excitation and now reduces to the time taken for a single dipole formation. The method so far implemented on various parallel architectures has the capacity to cater for photoionization calculations involving 500 - 1000 levels. This dramatically improves (a) the residual ion structure, (b) ionization potential, (c) resonance structure and (d) can deal with in excess of 5,000 close-coupled channels.

3 Scalability

As regards the scalability of our R-matrix codes, we find from experience on a variety of peta-flop architectures that various modules within this suite of codes scale well, upwards to 100,000 cores. In practical calculations for cross sections on various systems it is necessary to perform fine energy resolution of resonance features ($10^{-8} \text{ Ry} \sim 1.36 \text{ meV}$) observed in photoionization cross sections. This involves many (6 - 30 million) incident photon energies, vital when comparing with high precision measurements, like those for Xe^+ ions made at the Advanced Light Source synchrotron radiation facility in Berkeley, California, USA where energy resolutions of 4 meV FWHM are achieved [5].

The formation of many real symmetric matrices (Hamiltonians), typically 60 K -150 K, requires anywhere from 10-500 Gb of storage. The diagonalization of each matrix, from which *every* eigenvalue and *every* eigenvector is required is achieved through use of the ScaLapack package. In particular routines : **pdsyevx** and **pdsyevd**, where preference is given to the latter, as it ensures orthogonality between all eigenvectors. In typical collision calculations, matrices vary in size from $2\text{K} \times 2\text{K}$ to $200\text{K} \times 200 \text{ K}$, depending on the complexity of the atomic target. The formation of the continuum-continuum part of the N+1 electron Hamiltonian is the

most time consuming. Therefore if there are several thousand scattering channels ($nchan$) then there are $[nchan \times (nchan + 1)/2]$ matrix blocks. Each block represents a partial wave and each subgroup reads a single Hamiltonian and diagonalizes it in parallel, concurrently with each other. So there is endless scalability. R-matrix close-coupling calculations are therefore reduced to the time required for a single partial wave.

Optimization of the R-matrix codes on a variety of HPC architectures implements several good coding practices. We use code inlining (which reduces overhead from calling subroutines), loop unrolling, modularization, unit strides, vectorization and dynamic array passing. Highly optimized libraries such as; ScaLapack, BLAS and BLACS are used extensively in the codes, which are available at HLRS. On Cray architectures, such as the Cray-XE6 at Stuttgart, the R-matrix codes were profiled with performance utilities such as CrayPat which gives the user an indication of their scalability. Standard MPI/FORTRAN 90/95 programming is used on the world's leading-edge peta-flop high performance supercomputers. Serial (legacy) code to parallel R-matrix implementation is carried out using a small subset of basic MPI commands.

In Table 1 we show details of test runs for the outer region module PSTBF0DAMP for K-shell photoionization of B^+ using 249-coupled states with 400 coupled channels and 409,600 energy points and an increasing number of CPU cores. A factor of 4 speed up is achieved by using up to 8192 cores. The computations were carried out on the Cray-XE6 (Hopper) at NERSC, comparable to the Hermit architecture at HLRS, Stuttgart using the CrayPat utility. Note, for actual production runs, timings would be a factor of 10 larger, as one would require a mesh of 4,096,000 energy points to fully resolve the resonances features observed in the spectrum [8]. We present the timings for core sizes varying from 1024 to 8192 again for B^+ K-shell photoionization in its ground state. The computations were performed with the outer region module PSTGBF0DAMP for 249-states and 400-coupled channels. The main

Table 1 B^+ , 249-states, 400 coupled channels, 409,600 energy points running on an increasing number of cores. The results are from the module PSTGB0FDAMP for the photoionization cross-section calculations of ground state of the B^+ ion carried out on the Hopper architectures at NERSC comparable to Hermit at HLRS. Results presented illustrate the speed up factor with increasing number of CPU cores and the total number of core hours.

CRAY-XE6 CPU cores	Hopper (NERSC) Absolute timing (s)	Hopper (NERSC) Speed Up Factor	Hopper (NERSC) Total Core Hours
1024	584.19	1.0000	166.1155
2048	430.80	1.3584	245.0077
4096	223.08	2.6183	253.8154
8192	149.70	3.9018	340.6506

work horse in our linear algebra code is the ScaLAPACK libraries. The goals of the

ScaLAPACK project are the same as those of LAPACK; Efficiency (to run as fast as possible), Scalability (as the problem size grows so do the numbers of processors grow), Reliability (including error bounds), Flexibility (so users can construct new routines from well-designed parts) and Ease of Use (by making the interface to LAPACK and ScaLAPACK look as similar as possible). Many of these goals, particularly portability are aided by developing and promoting standards, especially for low level communication and computation routines.

Access to the Cray-XE6 at HLRS, January 2013 - May 2013, was provided for exploratory computations, to test our parallel Breit-Pauli and DARC codes. During this period, Connor Ballance and Brendan McLaughlin, worked closely with Stefan Andersson, the resident Cray Research consultant at HLRS, profiling and benchmarking our codes on this Cray-XE6. A variety of different detailed calculations were made on the Cray-XE6 HLRS architecture (Hermit) resulting in several publications [11, 14, 15]. A formal proposal was submitted to HLRS in June 2013 for access to this architecture for a project lead by Professor Alfred Müller from the University of Giessen.

4 X-ray and Inner-Shell Processes

4.1 Atomic Oxygen

An accurate description of the photoionization/photoabsorption of atomic oxygen is important for a number of atmospheric and astrophysical applications. Photo-absorption of atomic oxygen in the energy region below the $1s^{-1}$ threshold in X-ray spectroscopy from *Chandra* and *XMM-Newton* is observed in a variety of X-ray binary spectra. Photo-absorption cross sections determined from an R-matrix method with pseudo-states (RMPS) and high precision measurements from the Advanced Light Source (ALS) are presented in Fig. 1. High-resolution spectroscopy with $E/\Delta E \approx 4,250 \pm 400$ were obtained for photon energies from 520 eV to 555 eV at an energy resolution of 124 ± 12 meV FWHM. *K*-shell photoabsorption cross-section measurements were made on atomic oxygen at the ALS. Natural line widths Γ are extracted for the $1s^{-1}2s^22p^4(^4P)np^3P^\circ$ and $1s^{-1}2s^22p^4(^2P)np^3P^\circ$ Rydberg resonances series and compared with theoretical predictions. Accurate cross sections and line widths are obtained for applications in X-ray astronomy. Excellent agreement between theory and the ALS measurements is shown which will have profound implications for the modelling of X-ray spectra and spectral diagnostics. Further details can be found in our recent study on this complex [11].

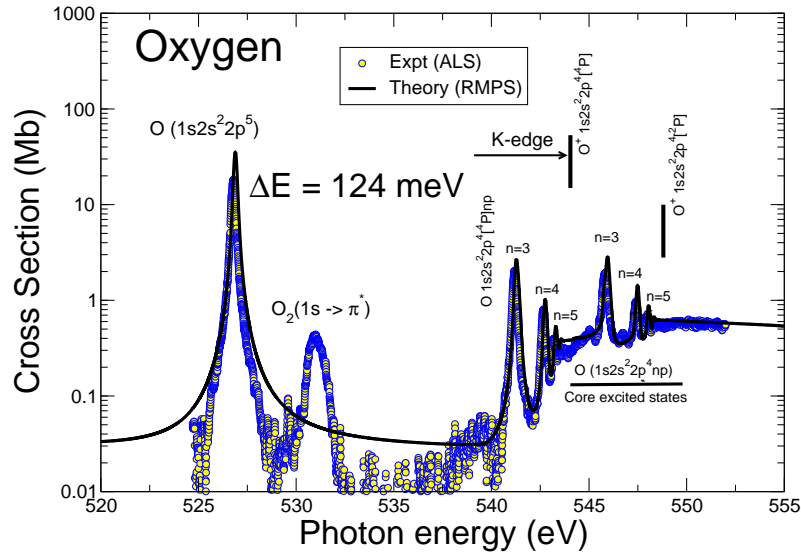


Fig. 1 (Colour online) Atomic oxygen photo-absorption cross sections taken at 124 meV FWHM compared with theoretical estimates. The R-matrix calculations shown are from the R-matrix with pseudo-states method (RMPS: solid black line, present results) convoluted with a Gaussian profile of 124 meV FWHM [11].

4.2 Nitrogen ions

Recent studies on *K*-shell photoionization of neutral nitrogen and oxygen showed excellent agreement with high resolution measurements made at the Advanced Light Source (ALS) radiation facility [11, 10] as have similar cross section calculations on singly and multiply ionized stages of atomic nitrogen compared with high resolution measurements at the SOLEIL synchrotron facility [13, 14, 15]. The majority of the high-resolution experimental data from third generation light sources show excellent agreement with the state-of-the-art R-matrix method and with other modern theoretical approaches.

The investigations on Li-like, Be-like and B-like atomic nitrogen ions gives accurate values of photoionization cross sections produced by X-rays in the vicinity of the *K*-edge, where strong $n=2$ inner-shell resonance states are observed. N^{2+} ions produced in the SOLEIL synchrotron radiation experiments are not purely in their ground state (see Figure 2). *K*-shell photoionization contributes to the ionization balance in a more complicated way than outer shell photoionization. In fact *K*-shell

photoionization when followed by Auger decay couples three or more ionization stages instead of two in the usual equations of ionization equilibrium [14, 15].

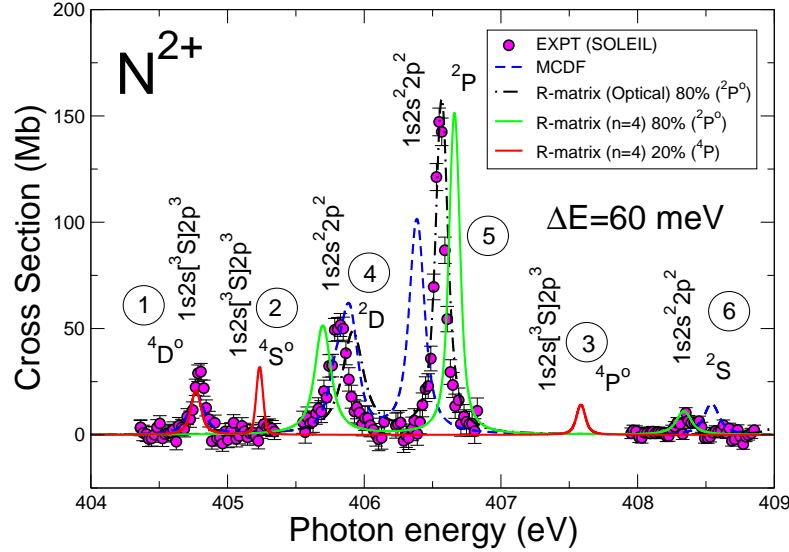


Fig. 2 (Colour online) Photoionization cross sections for N^{2+} ions measured with a 60 meV band pass at SOLEIL. Solid circles : total photoionization. The error bars give the statistical uncertainty of the experimental data. The MCDF (dashed line), R-matrix RMPS (solid line, red, 4P , green, $^2P^o$), and the Optical potential (dash-dot line, $^2P^o$ only) calculations shown were obtained by convolution with a Gaussian distribution having a profile width at FWHM of 60 meV and a weighting of the ground and metastable states to simulate the measurements [15].

The R-matrix with pseudo-states method (RMPS) was used to determine all the cross sections (in LS - coupling) with 390 levels of the N^{3+} residual ion included in the close-coupling calculations. Since metastable states are present in the parent ion beam, theoretical PI cross-section calculations are required for both the $1s^22s^22p^2\ ^2P^o$ ground state and the $1s^22s2p^2\ ^4P$ metastable states of the N^{2+} ion for a proper comparison with experiment. The scattering wavefunctions were generated by allowing two-electron promotions out of selected base configurations of N^{2+} . Scattering calculations were performed with twenty continuum functions and a boundary radius of 9.4 Bohr radii. For the $^2P^o$ ground state and the 4P metastable states the electron-ion collision problem was solved with a fine energy mesh of 2×10^{-7} Rydbergs ($\approx 2.72\ \mu\text{eV}$) to delineate all the resonance features in the PI

cross sections. Radiation and Auger damping were also included in the cross section calculations.

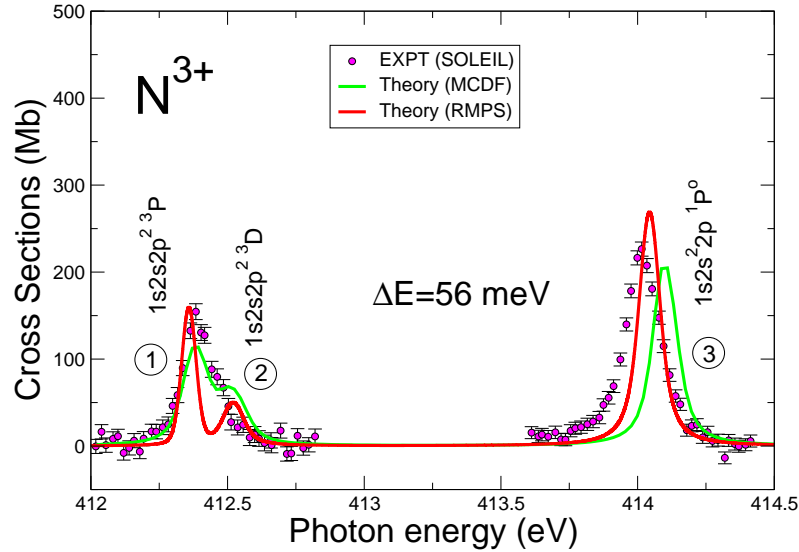


Fig. 3 (Colour online) Photoionization cross sections for Be-like atomic nitrogen (N^{3+}) ions measured with a 56 meV band pass at the SOLEIL radiation facility. Solid circles : total photoionization. The error bars give the statistical uncertainty of the experimental data. The MCDF (solid green line) and R-matrix (solid red line) calculations shown are convoluted with a Gaussian profile of 56 meV FWHM and an appropriate weighting of the ground and metastable states to simulate the measurements. For the metastable ${}^3P^\circ$ state, the MCDF calculations have been shifted up by +1.46 eV in order to match experiment. [14].

For a direct comparison with the SOLEIL results, the R-matrix cross section calculations were convoluted with a Gaussian function of appropriate width and an admixture of 80% ground and 20% metastable states used to best simulate experiment. The peaks found in the theoretical photoionization cross section spectrum were fitted to Fano profiles for overlapping resonances as opposed to the energy derivative of the eigenphase sum method [14, 15].

For Be-like ions both the initial 1S ground state and the ${}^3P^\circ$ metastable states were required (see Figure 3). Cross section calculations were carried out in LS -coupling with 390-levels retained in the close-coupling expansion using the R-matrix with pseudo states method (RMPS). The Hartree-Fock $1s$, $2s$ and $2p$ were used with $n=3$ physical and $n=4$ pseudo orbitals of the residual N^{4+} ion. The $n=4$ pseudo-

orbitals were determined by energy optimization on the ground state of the N^{4+} ion, with the atomic structure code CIV3. The N^{4+} residual 390 ion states used multi-configuration interaction target wave functions. The non-relativistic R -matrix method determined the energies of the N^{3+} bound states and all the appropriate cross sections. We determined PI cross sections for the $1s^2 2s^2 \ ^1S$ ground state and the $1s^2 2s 2p \ ^3P^o$ metastable state.

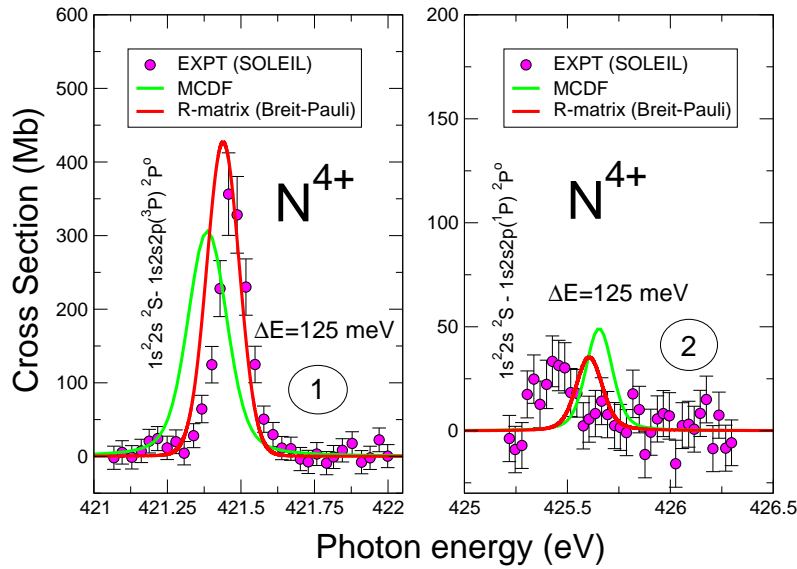


Fig. 4 (Colour online) Photoionization cross sections for Li-like atomic nitrogen (N^{4+}) ions measured with a 125 meV FWHM band pass at the SOLEIL radiation facility. Solid circles : absolute total photoionization cross sections. The error bars give the statistical uncertainty of the experimental data. R-matrix (solid red line, 31 levels) intermediate coupling, MCDF (solid green line), calculations shown are convolution with a Gaussian profile of 125 meV FWHM to simulate the measurements [14].

For Li-like systems, intermediate-coupling photoionization cross section calculations were performed using the semi-relativistic Breit-Pauli approximation (see Figure 4). An appropriate number of N^{5+} residual ion states (19 LS , 31 LSJ levels) were included in our intermediate coupling calculations. The $n=4$ basis set of N^{3+} orbitals obtained from the atomic-structure code CIV3 were used to represent the wave-functions. Photoionization cross-section calculations were then performed in intermediate coupling for the $1s^2 2s^2 \ ^2S_{1/2}$ initial state of the N^{4+} ion in order to incorporate relativistic effects via the semi-relativistic Breit-Pauli approximation.

For cross section calculations, He-like LS states were retained: $1s^2\ ^1S$, $1sns\ ^{1,3}S$, $1snp\ ^{1,3}P^\circ$, $1snd\ ^{1,3}D$, and $1snf\ ^{1,3}F^\circ$, $n \leq 4$, of the N^{5+} ion core giving rise to 31 LSJ states in the intermediate close-coupling expansions for the $J=1/2$ initial scattering symmetry of the Li-like N^{4+} ion. The $n=4$ pseudo states are included in an attempt to model core relaxation, electron correlations effects and the infinite number of states (bound and continuum) left out by the truncation of the close-coupling expansion in our work. For the structure calculations of the residual N^{5+} ion, all $n=3$ physical orbitals and $n=4$ correlation orbitals were included in the multi-configuration-interaction target wave-functions expansions used to describe the states.

5 Heavy atomic systems

5.1 Xe ions

Photoionization cross sections of heavy atomic elements, in low stages of ionization, are currently of interest both experimentally and theoretically and for applications in astrophysics. The data from such processes have many applications in planetary nebulae, where they are of use in identifying weak emission lines of n -capture elements in NGC 3242.

Xenon ions are of importance in man-made plasmas such as XUV light sources for semiconductor lithography, ion thrusters for space craft propulsion and nuclear fusion plasmas. Xenon ions have also been detected in cosmic objects, e.g., in several planetary nebulae and in the ejected envelopes of low- and intermediate-mass stars [5]. Collision processes with highly charged xenon ions are of interest for UV-radiation generation in plasma discharges, for fusion research and for space craft propulsion. Here we report theoretical and experimental results for the photoionization of Ag-like (Xe^{7+}) xenon ions which were measured at the photon-ion end station of ALS on beamline 10.0.1. Compared with the only previous experimental study of Bizau and co-workers [17] of this reaction, the present cross-sections were obtained at higher energy resolution (38 – 100 meV versus 200 – 500 meV) and on an absolute cross-section scale. In the experimental photon energy range of 95 – 145 eV the cross-section is dominated by resonances associated with $4d \rightarrow 5f$ excitation and subsequent autoionization. The theoretical results were obtained using the Dirac Coulomb R-matrix approximation [16, 5, 12]. The small resonances below the ground-state ionization threshold, located at about 106 eV [18], are due to the presence of metastable $Xe^{7+}(4d^{10}4f^2F_{5/2,7/2}^\circ)$ ions with an excitation energy of 32.9 eV [18] in the ion beam. In the experimental photon energy range of 95 – 145 eV the cross-section is dominated by resonances associated with $4d \rightarrow 5f$ excitation and subsequent autoionization. The most prominent feature in the measured spectrum is the giant $4d^95s5f^2P^\circ$ resonance located at 122.139 ± 0.01 eV, which reaches a peak cross-section of 1.2 Gb at 38 meV photon energy spread [19]. The

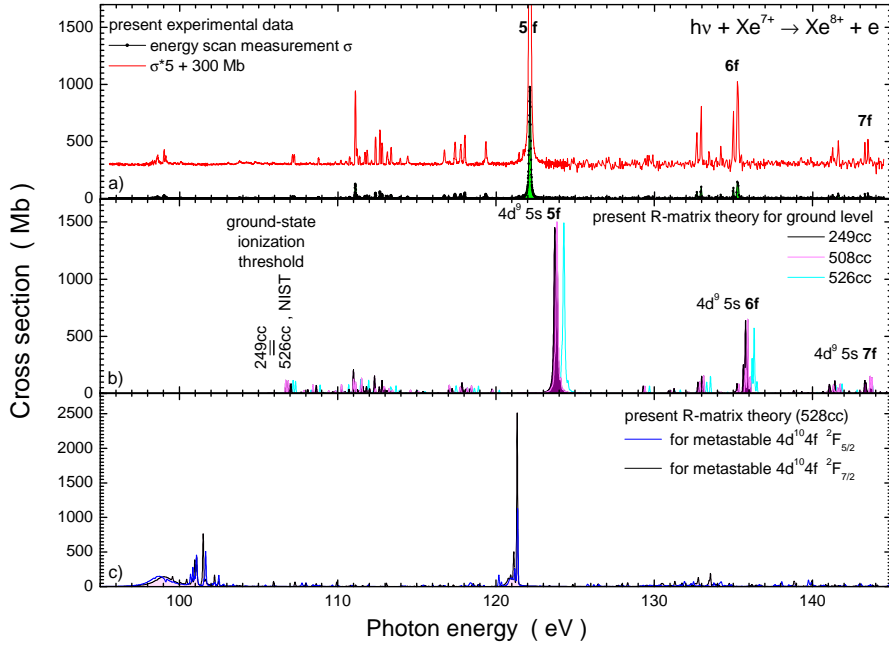


Fig. 5 (Colour online) The experimental and theoretical results of the present study of photoionization of Xe^{7+} ions. The top (panel a) displays the experimental energy-scan data taken at 65 meV resolution (data points connected by straight lines with light shading). In order to visualize the contributions of resonances other than the dominating $4d^9 5s 5f \ ^2P^o$ peak, the experimental data were multiplied by a factor of 5 and offset by 300 Mb (solid line, red online). Panel b) displays the present DARC results for a 249-level, a 508-level and a 526-level calculation, abbreviated as 249cc, 508cc and 526cc, respectively, for photoionization of ground-state Xe^{7+} ions. Panel c) shows 528-level DARC results for the two metastable fine-structure components of the long lived excited $4d^{10} 4f \ ^2F^o$ term. The theoretical cross sections were convoluted with a 65 meV FWHM Gaussian in order to be comparable with the experiment.

experimental resonance strength of (161 ± 31) Mb eV (corresponding to an absorption oscillator strength of 1.47 ± 0.28), width of 76 ± 3 meV, is in suitable agreement with the present theoretical estimate and with previous investigations [17]. The high-precision cross-section measurements obtained from the Advanced Light source compared with large-scale theoretical calculations obtained from a Dirac Coulomb R-matrix approach over the entire photon energy region investigated show suitable agreement.

The present work on Ag-like ions of Xenon provides a benchmark for future work. In addition to the direct photoionization process, indirect excitation processes occur for the interaction of a photon with the $4d^{10} 5s \ ^2S_{1/2}$ ground-state and the metastable $4d^{10} 4f \ ^2F_{5/2,7/2}^o$ levels of the Xe^{7+} ion. These intermediate resonance states can then decay to the ground state or energy accessible excited states.

Photoionization cross-sections on this complex ion were performed for the ground ($4d^{10}5s$) and the excited metastable ($4d^{10}4f$) levels associated with the Ag-like xenon ion to benchmark our theoretical results with the present high resolution experimental measurements made at the Advanced Light Source radiation facility in Berkeley [20]. The atomic structure calculations were carried out using the GRASP code. Initial scattering calculations were performed using 249-levels arising from twelve configurations of the Pd-like (Xe^{8+}) residual ion. Further collision models were investigated where both a 508-level and 526-level approximation were used in the close-coupling calculations. For the $4d^{10}4f^2F_{7/2,5/2}$ metastable states of this ion, both a 249-level and a 528-level model were investigated [20].

Photoionization cross-section calculations were performed in the Dirac Coulomb approximation using the DARC codes [16, 5, 12] for different scattering models for the ground $4d^{10}5s^2S_{1/2}$ state of the Xe^{7+} ion. The R-matrix boundary radius of 12.03 Bohr radii was sufficient to envelop the radial extent of all the $n=6$ atomic orbitals of the residual Xe^{7+} ion. A basis of 16 continuum orbitals was sufficient to span the incident experimental photon energy range from threshold up to 150 eV. Dipole selection rules for the ground-state photoionization require only the bound-free dipole matrices, $2J^\pi = 1^e \rightarrow 2J^\pi = 1^o, 3^o$. For the excited metastable states, $2J^\pi = 5^o \rightarrow 2J^\pi = 3^e, 5^e, 7^e$ and $2J^\pi = 7^o \rightarrow 2J^\pi = 5^e, 7^e, 9^e$ are necessary.

In the experimental photon energy range of 95 – 145 eV the cross-section is dominated by resonances associated with $4d \rightarrow 5f$ excitation and subsequent autoionization. We performed 249-level, 508-level and 526-level DARC photoionization cross-section calculations for the $\text{Xe}^{7+}(4d^{10}5s^2S_{1/2})$ ground state to check on the convergence of our results. Figure 5, includes the theoretical cross-sections results from the 249-state, 508-state, 526-state and 528-state models, compared to experiment. We find best agreement with experiment from an admixture of 97.6% ground and 2.4% metastable state. Given the complexity of this system, satisfactory agreement with experiment is obtained over the photon energy region investigated. We see that the small resonances below the ground-state ionization threshold, occurring at about 106 eV [18], are due to the presence of metastable $\text{Xe}^{7+}(4d^{10}4f^2F_{5/2,7/2}^o)$ ions with an excitation energy of 32.9 eV [18] in the ion beam.

Recently, the photon-ion merged-beams technique has been employed at the new Photon-Ion spectrometer at PETRA III (PIPE), in Hamburg, Germany, for measuring multiple photoionization of Xe^{q+} ($q=1-5$) ions [22]. Prominent ionization features have been observed in the photon-energy range 650 – 800 eV, which are associated with excitation or ionization of an inner-shell 3d electron. Large-scale DARC calculations are planned for the various charged states of these Xe ions.

5.2 Tungsten (W) Ions

The choice of materials for the plasma facing components in fusion experiments is guided by competing desirables: on the one hand the material should have a high thermal conductivity, high threshold for melting and sputtering, and low erosion

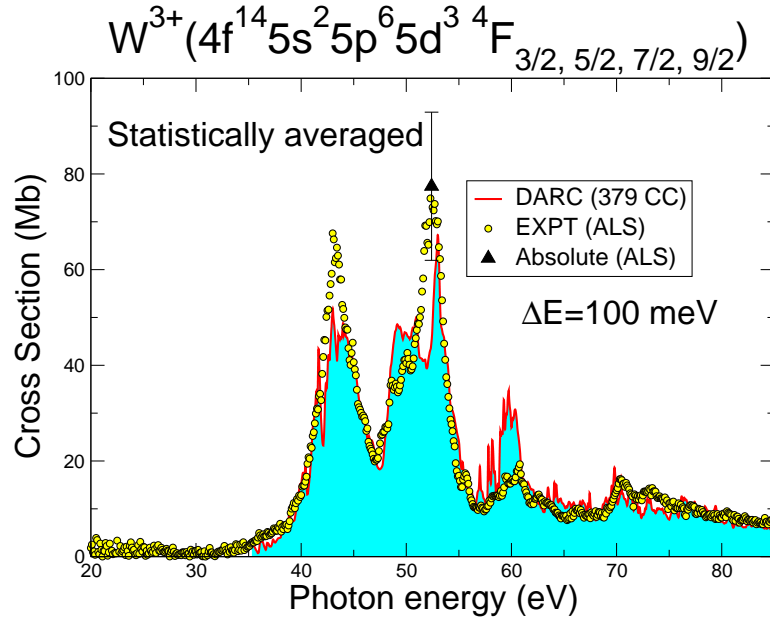


Fig. 6 Photoionization of W^{3+} ions over the photon energy range 20 eV - 90 eV. Theoretical work (solid red line: DARC) from the 379-level approximation calculations, convoluted with a Gaussian profile of 100 meV FWHM and statistically averaged over the fine structure $J = 3/2, 5/2, 7/2$ and $9/2$ levels. The solid circles (yellow) are from the experimental measurements made at the ALS using a band width of 100 meV [21]. The solid triangle is the absolute photoionization cross section accurate to within 20%.

rate under plasma contact, and on the other hand as a plasma impurity it should not cause excessive radiative energy loss. The default choice of material for present experiments is carbon (or graphite), however tritium is easily trapped in carbon-based walls and for that reason carbon is at present held to be unacceptable for use in a D-T fusion experiment such as ITER. In its place, tungsten (symbol W, atomic number 74) is the favoured material for the wall regions of highest particle and heat load in a fusion reactor vessel.

ITER is scheduled to start operation with a W-Be-C wall for a brief initial campaign before switching to W-Be or W alone for the main D-D and D-T experimental program. The attractiveness of tungsten is due to its high thermal conductivity, its high melting point, and its resistance to sputtering and erosion, and is in spite of a severe negative factor (that as a high-Z plasma impurity tungsten) does not become fully stripped of electrons and radiate copiously, so that the tolerable fraction of tungsten impurity in the plasma is at most 2×10^{-5} .

W ions impurities in a fusion plasma causes critical radiation loss and minuscule concentrations prevent ignition. High resolution experiments are currently available from the ALS on low ionization stages of W ions. We use the Dirac-Atomic-R-matrix-Codes (DARC) to perform large scale calculations for the single photoionization process and compare our results with experiment. These systems are an excellent test bed for the photoionization (PI) process where excellent agreement is achieved between theory and experiment providing a road-map for electron - impact excitation (EIE). For photoionization of the W^{3+} ion of tungsten we use a 379 – level scattering model, obtained from 9 configuration state functions of the residual ion. Figure 6 shows our theoretical results from this 379-level model obtained from the DARC codes compared with measurements made at the Advanced Light source [21]. The comparison made in Figure 6 illustrates suitable agreement between the theoretical results and the ALS experimental measurements which are accurate to within 20%.

Acknowledgements A Müller acknowledges support by Deutsche Forschungsgemeinschaft under project number Mu 1068/10 and through NATO Collaborative Linkage grant 976362 as well as by the US Department of Energy (DOE) under contract DE-AC03-76SF-00098 and grant DE-FG02-03ER15424. M S Pindzola and C P Ballance were supported by US Department of Energy (DOE) and US National Science Foundation grants through Auburn University. B M McLaughlin acknowledges support from the US National Science Foundation through a grant to ITAMP at the Harvard-Smithsonian Center for Astrophysics, under the visitor’s program, the RTRA network *Triangle de le Physique* and a visiting research fellowship (VRF) from Queen’s University Belfast. This research used computational resources at the National Energy Research Scientific Computing Center in Oakland, CA, USA, the Kraken XT5 facility at the National Institute for Computational Science (NICS) in Knoxville, TN, USA and at the High Performance Computing Center Stuttgart (HLRS) of the University of Stuttgart, Stuttgart, Germany. The Kraken XT5 facility is a resource of the Extreme Science and Engineering Discovery Environment (XSEDE), which is supported by National Science Foundation grant number OCI-1053575. The Oak Ridge Leadership Computing Facility at the Oak Ridge National Laboratory, provided additional computational resources, which is supported by the Office of Science of the U.S. Department of Energy under Contract No. DE-AC05-00OR22725. The Advanced Light Source is supported by the Director, Office of Science, Office of Basic Energy Sciences, of the US Department of Energy under Contract No. DE-AC02-05CH11231.

References

1. McLaughlin, B. M.: Inner-shell Photoionization, Fluorescence and Auger Yields. In: Ferland, G. and Savin, D. W. (eds) Spectroscopic Challenges of Photoionized Plasma, Astronomical Society of the Pacific, ASP Conf. Series **247** pp. 87. San Francisco (2001)
2. Kallman, T. R.: Challenges of Plasma Modelling: Current Status and Future Plans. Space Sci. Rev. **157**, 177 (2010)
3. McLaughlin, B. M. and Ballance, C. P.: Photoionization, Fluorescence and Inner-shell Processes. In: McGraw-Hill (eds) McGraw-Hill Yearbook of Science and Technology, pp. 281. McGraw Hill, New York (2013)
4. Hasoglu, M. F., Abdel Naby S. A., Gorczyca, T. W., Drake J. J. and McLaughlin, B. M. : K-shell Photoabsorption Studies of the Carbon Isonuclear Sequence. *Astrophys. J.* **724**, 1296 (2010)
5. McLaughlin, B. M. and Ballance, C. P.: Photoionization cross section calculations for the halogen-like ions Kr^+ and Xe^+ . *J. Phys. B: At. Mol. Opt. Phys.* **45**, 085701 (2012)
6. Ballance, C. P., and Griffin D. C.: Relativistic radiatively damped R-matrix calculation of the electron-impact excitation of W^{46+} . *J. Phys. B: At. Mol. Opt. Phys.* **39**, 3617 (2006)
7. Ballance, C. P., Loch S. D., Pindzola M. S. and Griffin D. C.: Electron-impact excitation and ionization of W^{3+} for the determination of tungsten influx in a fusion plasma. *J. Phys. B: At. Mol. Opt. Phys.* **46**, 055202 (2013)
8. Müller, A., Schippers, S., Phaneuf, R. A., Scully, S. W. J., Aguilar, A., Cisneros, C., Gharaibeh, M. F., Schlachter, A. S., and McLaughlin, B. M.: K-shell photoionization of Be-like Boron (B^+) Ions: Experiment and Theory *J. Phys. B: At. Mol. Opt. Phys.* **47**, 135201 (2014)
9. Covington, A. M., Aguilar, A., Covington, I. R., Hinojosa, G., Shirley, C. A., Phaneuf, R. A., Álvarez, I., Cisneros, C., Dominguez-Lopez, I., Sant'Anna, M. M., Schlachter, A. S., Ballance, C. P. and McLaughlin, B. M.: Valence-shell photoionization of chlorinelike Ar^+ ions. *Phys. Rev. A* **84**, 013413 (2011)
10. Sant'Anna, M. M., Schlachter, A. S., Öhrwall, G., Stolte, W. C., Lindle, D. W. and McLaughlin, B. M.: K-shell X-ray Spectroscopy of Atomic Nitrogen. *Phys. Rev. Lett.* **107**, 033001 (2011)
11. McLaughlin, B. M., Ballance, C. P., Bown, K. P., Gardenghi, D. J. and Stolte, W. C.: High Precision K-shell Photoabsorption Cross Sections for Atomic Oxygen: Experiment and Theory. *Astrophys. J.* **771**, L8 (2013) & **779**, L31 (2013)
12. McLaughlin, B. M. and Ballance, C. P.: Photoionization Cross-Sections for the trans-iron element Se^+ from 18 eV to 31 eV. *J. Phys. B: At. Mol. Opt. Phys.* **45**, 095202 (2012)
13. Gharaibeh, M. F., Bizau, J. M., Cubaynes, D., Guilbaud, S., El Hassan, N., Al Shorman, M. M., Miron, C., Nicolas, C., Robert, E., Blancard, C. and McLaughlin, B. M.: K-shell photoionization of singly ionized atomic nitrogen: experiment and theory. *J. Phys. B: At. Mol. Opt. Phys.* **44**, 175208 (2011)
14. Al Shorman, M. M., Gharaibeh, M. F., Bizau, J. M., Cubaynes, D., Guilbaud, S., El Hassan, N., Miron, C., Nicolas, C., Robert, E., Sakho, I, Blancard, C. and McLaughlin, B. M.: K-Shell Photoionization of Be-like and Li-like Ions of atomic nitrogen: experiment and theory. *J. Phys. B: At. Mol. Opt. Phys.* **46**, 195701 (2013)
15. Gharaibeh, M. F., El Hassan, N., Al Shorman, M. M., Bizau, J. M., Cubaynes, D., Guilbaud, S., Blancard, C. and McLaughlin, B. M.: K-shell photoionization of B-like atomic nitrogen ions: experiment and theory. *J. Phys. B: At. Mol. Opt. Phys.* **47**, 065201 (2014)
16. Fivet, V., Bautista, M. A. and Ballance, C. P.: Fine-structure photoionization cross sections of Fe II. *J. Phys. B: At. Mol. Opt. Phys.* **45**, 035201 (2012)
17. Bizau, J. M., Esteve, J.-M., Cubaynes, D., Wuilleumier, F. J, Blancard, C., Compant La Fontaine, A., Couillaud, C., Lachkar, J., Marmoret, R., Rmond, C., Bruneau, J., Hitz, D., Ludwig, P., and Delaunay, M. : Photoionization of Highly Charged Ions Using an ECR Ion Source and Undulator Radiation. *Phys. Rev. Letts.* **84**, 435 (2000)
18. Saloman, E. B. : Energy Levels and Observed Spectral Lines of Xenon, Xe I through Xe LIV. *J. Phys. Chem. Ref. Data* **33**, 765 (2004)

19. Schippers, S., Müller, A., Esteves, D., Habibi, M., Aguilar, A. and Kilcoyne, A. L. D. : Experimental absolute cross section for photoionization of Xe^{7+} . J. Phys. Conf. Ser. **194**, 022094 (2009)
20. Müller, A., Schippers, S., Esteves-Macaluso, D., Habibi, M., Aguilar, A., Kilcoyne, A. L. D., Phaneuf, R. A., Ballance, C. P. and McLaughlin, B. M.: High Resolution Valence shell Photoionization of Ag-like (Xe^{7+}) Xenon ions : Experiment and Theory. J. Phys. B: At. Mol. Opt. Phys., **47**, 215202 (2014)
21. McLaughlin, B. M., Ballance, C. P., Kilcoyne, A. L. D., Phaneuf, R. A., Hellhund, J., Schippers, S., and Müller, A.: Valence shell Photoionization of Hf-like (W^{2+}) and Lu-like (W^{3+}) ions of Atomic Tungsten : Experiment and Theory. J. Phys. B: At. Mol. Opt. Phys., *submitted for publication* (2014)
22. Schippers, S., Ricz, S., Buhr, T., Borovik Jr, A., Hellhund, J., Holste, K., Huber, K., SchLfer, H.-J., Schury, D., Klumpp, S., Mertens, K., Martins, M., Flesch, R., Ulrich, G., Rhl, E., Jahnke, T., Lower, J., Metz, D., Schmidt, L. P. H., Schffler, M., Williams, J. B., Glaser, L., Scholz, F., Seltmann, J., Viefhaus, J., Dorn, A., Wolf, A., Ullrich J. and Mller, A.: Absolute cross sections for photoionization of Xe^{q+} ions ($1 \leq q \leq 5$) at the $3d$ ionization threshold, J. Phys. B: At. Mol. Opt. Phys. **47**, 115602 (2014)